2014 IEEE International Conference on Fuzzy Systems (FUZZ-IEEE)
July 6-11, 2014, Beijing, China

Model based Lithium Ion cell ageing data analysis

Christoph Hametner, Wenzel Prochazka, Amra Suljanovic and Stefan Jakubek

Abstract— **This paper reports the model based analysis of Lithium Ion cell ageing and the age-related adaptation of data driven battery models is addressed. To take account of ageing is an important issue e. g. for the battery management of (hybrid) electrical vehicles, in order to provide an exact online estimate of the state of charge (SoC). As a first step, ageing data analysis based on the architecture of local model networks (LMNs) is presented using data from a large scale ageing experiment of Lithium Ion cells. Additionally, the topic of time-variant battery modelling is addressed. Thus, the LMN is adapted in a way that age-related effects (such as capacity decay and resistance increase) are taken into account. Such a model can further be used for the design of a combined observer for SoC and state of health (SoH).**

Index Terms— **Nonlinear system identification, battery ageing, fuzzy observer, state of charge, state of health**

I. Introduction

AGEING performance testing of Lithium Ion cells and the associated model parameterisation as well as studies on ageing mechanisms have become an increasingly important issue in recent years. In this paper, the model based analysis of Lithium Ion cell ageing data is presented and the age-related adaptation of data driven battery models for state of charge (SoC) estimation is addressed. Especially in hybrid electrical vehicles (HEVs), an accurate observation of the electric power supply is essential in order to extend battery life and preserve the usable capacity. Accordingly, a proper *online* monitoring of the SoC of the battery is required. Since the SoC cannot be measured directly, the SoC *estimation* is one of the most important functions of the battery management system (BMS).

Various publications have addressed the design of nonlinear SoC observers, see e. g. [1], [2], [3], [4]. Typically, SoC estimation is based on a nonlinear model using Kalman filter theory. In [5] the modelling and identification of a state space structure which includes terms that describe the dynamic contributions due to open-circuit voltage, ohmic loss, polarization time constants is described and the SoC estimation using an extended Kalman filter (EKF) is proposed. The online estimation of the SoC of a lithium ion cell based on an electrochemical model can be found in [6]. In [7] a simple resistor-capacitor battery model is used where modelling errors caused by the simple model are compensated by a sliding mode observer. However, in order to allow for the application of such observers in an HEV, the actual state of health (SoH) of the cell also has to be estimated *online* and considered as well for SoC estimation. Without an SoH correction or update by the BMS, the driver will experience an overestimated range or less acceleration, [8]. Recent publications have addressed the design of a *combined* observer for SoC and SoH. In e. g. [8] the design of a dual filter consisting of a standard Kalman filter and an unscented Kalman filter based on an equivalent circuit model is presented. The SoH estimation of valve regulated lead-acid cells using an equivalent circuit model and an EKF is described in [9]. However, conventional physical modelling and/or time efficient parameterisation of these models is difficult in many situations. To overcome such problems, in [10] the authors presented a systematic approach for *data driven* modelling and the associated nonlinear observer design for SoC estimation. An important advantage in this context is that such a purely data driven methodology is not limited to a certain battery type/chemistry. In [10] the proposed concepts were validated by means of real measurement data from a Lithium Ion cell. Using a fuzzy observer architecture an accurate estimation of the SoC is obtained and the computational complexity of the global filter is greatly reduced compared to the widely used EKF. While such a data driven approach enables the application for any type of battery chemistry, a major disadvantage of these black-box models is that the physical interpretation of the model parameters is not easily possible. In the present paper, the adaptation of data driven black-box models is addressed since, for the design of a combined observer for SoH and SoC, a model which takes the age-related capacity decay and/or internal resistance increase into account, is required.

A schematics of a cascaded observer structure for simultaneous SoH and SoC estimation is depicted in Fig. 1. The inner loop represents the fuzzy observer for SoC estimation, where the correction is obtained from a comparison of the actual (measured) terminal voltage of the battery to the output of the local model network (LMN), see [10]. The outer loop represents the SoH observer, which estimates the currently available cell capacity $\hat{C}_{act}$. Thus, the LMN has to be *adapted* in a way, that the capacity decay of the cell is taken into account. The actual design of the combined (cascaded) observer and its convergence analysis are not addressed in this paper and subject of current research.

In the present paper, as a first step, the model based analysis of Lithium Ion cell ageing data is presented and adaptation of the battery model (the LMN) is addressed. For model based ageing data analysis, the interpretability of

Christoph Hametner and Stefan Jakubek are with the Christian Doppler Laboratory for Model Based Calibration Methodologies, Vienna University of Technology, 1040 Vienna, Austria (email: {christoph.hametner, stefan.jakubek}@tuwien.ac.at).

Wenzel Prochazka and Amra Suljanovic are with the AVL List GmbH, 8020 Graz, Austria (email: {wenzel.prochazka, amra.suljanovic}@avl.com).

This work was supported by the Christian Doppler Research Association and AVL List GmbH, Graz. Further, for all measurements shown in this work, the authors would like to thank the Virtual Vehicle Competence and Test Center and to acknowledge the financial support thereof by the Austrian "COMET K2 - Competence Centers for Excellent Technologies Program".

978-1-4799-2072-3/14/$31.00

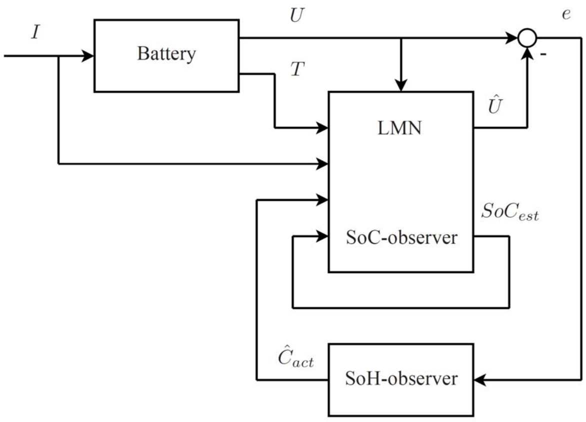

Fig. 1. Schematics of a combined observer for SoC and SoH

LMNs is of great interest in order to extract information on the power fade (internal resistance) and capacity fade (energy content). For that purpose, data from a large scale ageing experiment [11] are used. In [11] the experiment design for ageing of Lithium Ion cells is described and the capacity loss of lab-size Lithium Ion cells is studied to give a more consistent picture of the cell ageing process.

The remainder of this paper is structured as follows: In Section II the architecture of LMNs is shortly reviewed. The LMN based analysis of ageing data is presented in Section III. The topic age-related model adaptation is addressed in Section IV.

II. Data driven battery modelling

This section briefly reviews the LMN architecture and the data driven construction of the battery model.

Since conventional physical modelling is difficult in many situations, black-box and grey-box-oriented nonlinear system identification procedures have emerged as a feasible alternative in various applications. In this context, LMNs have evidenced to be a powerful tool (see also e. g. [12], [13]) since they can adapt to the complexity of the problem in a highly efficient way. Especially in automotive applications, these data driven modelling approaches are an important tool for systematically dealing with the growing complexity of e. g. combustion engines and hybrid components, see [14], [15], [16].

An integral part of the SoC observer from [10] is a mathematical cell model (represented by the LMN), which describes the dynamic behaviour of the terminal voltage $U(t)$ based on the charge/discharge current $I(t)$ and other factors (e. g. temperature and SoC). The LMN interpolates between different local models, each of which are valid in a certain region of the input space. Thus, the battery cell model is based on a partitioning into several local operating regimes (local linear impedance models), represented by the dominant influence of the scheduling variables, such as SoC, temperature, etc. This strategy makes it possible to capture the highly nonlinear dynamic complexity of the battery in a computationally efficient way. Additionally, the architecture of LMNs represents an excellent approach for the integration of various knowledge sources. Accordingly, the complexity of the identification procedure can be reduced significantly when prior knowledge about the underlying system is available, see e. g. [16].

In general, each local model of the LMN - indicated by subscript i - consists of two parts: The *validity function* Φ_i and its *model parameter vector* $\boldsymbol{\theta}_i$. Thereby, Φ_i defines the region of validity of the i-th local model.

The *local* estimate for the output is obtained by

$$\hat{y}_i(k) = \boldsymbol{x}^T(k)\boldsymbol{\theta}_i, \tag{1}$$

where $\boldsymbol{x}^T(k)$ denotes the regressor vector. In dynamic system identification, the regressor vector $\boldsymbol{x}(k)$ comprises past system inputs and outputs.

All local estimations $\hat{y}_i(k)$ are used to form the global model output $\hat{y}(k)$ by weighted aggregation

$$\hat{y}(k) = \sum_{i=1}^{M} \Phi_i(\tilde{\boldsymbol{x}}(k))\hat{y}_i(k), \tag{2}$$

where M denotes the number of local linear models. Thereby, the elements in $\tilde{\boldsymbol{x}}(k)$ span the so-called partition space and are chosen on the basis of prior knowledge about the process and the expected structure of its nonlinearities.

The computation of the validity functions $\Phi_i(\tilde{\boldsymbol{x}}(k))$ is based on a logistic discriminant tree. In Fig. 2 a model tree with three local models is depicted. Each node corresponds to a split of the partition space into two parts, and the free ends of the branches represent the actual local models with their parameter vector $\boldsymbol{\theta}_i$ and their validity functions Φ_i. The overall nonlinear model thus comprises M local models and $M-1$ nodes that determine their regions of validity.

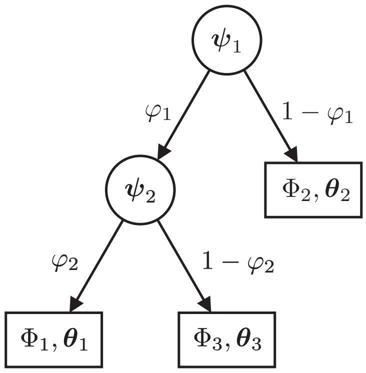

Fig. 2. Logistic discriminant tree

$$\Phi_1 = \varphi_1\varphi_2, \tag{3}$$

$$\Phi_2 = 1 - \varphi_1, \tag{4}$$

$$\Phi_3 = \varphi_1(1 - \varphi_2). \tag{5}$$

For the representation of the discriminant function in the d-th node, a logistic sigmoid activation function is chosen, c. f. [17]:

$$\varphi_d(\tilde{\boldsymbol{x}}(k)) = \frac{1}{1+\exp(-a_d(\tilde{\boldsymbol{x}}(k)))} \tag{6}$$

with

$$a_d(\tilde{\boldsymbol{x}}(k)) = \begin{bmatrix} 1 & \tilde{\boldsymbol{x}}^T(k) \end{bmatrix} \begin{bmatrix} \psi_{d0} \\ \tilde{\boldsymbol{\psi}}_d \end{bmatrix}. \tag{7}$$

Here, $\tilde{\boldsymbol{\psi}}_d^T = \begin{bmatrix} \psi_{d1} \dots & \psi_{dp} \end{bmatrix}$ denotes the weight vector, and ψ_{d0} is called the bias term. The discriminant functions φ_d are used to calculate the validity functions Φ_i, c. f. [18]. The validity functions for the layout in Fig. 2 are obtained by (3), (4) and (5).

The training (i.e. the parametrisation) of the battery model (the LMN) is then based on a nonlinear optimisation algorithm. For a more detailed description of the iterative optimisation algorithm, please refer to [19] and [15]. However, the results presented in [16] and [10] indicate the excellent generalisation capabilities of the proposed LMN training algorithm.

III. Model based ageing data analysis

This section describes the model based analysis of ageing data using the proposed LMN training algorithm.

A. Lithium Ion cell ageing data

Data from a large scale ageing experiment [11] are used to investigate how ageing affects the data driven battery model (see Section II). In [11] the experiment design of load cycles for Lithium Ion cell ageing tests is described. During these ageing tests, the cycling load as well as calender ageing was periodically interrupted by specially designed reference tests. For the cell chosen to be exemplary in this paper, 17 reference tests were recorded, each representing the cell at some stage of the ageing process. The temperature was kept constant for these tests and is thus not considered in this paper. Fig. 3 shows the age-related capacity decay C_{act}/C_{init} of the cell over time where each point represents one reference test.

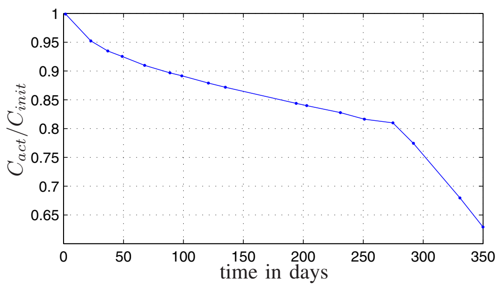

Fig. 3. Capacity decay over time

In addition, the capacity decay C_{act}/C_{init} over cycle count is shown in Fig. 4.

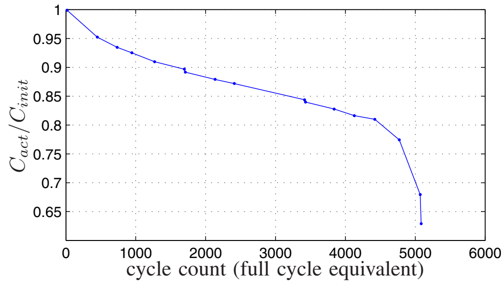

Fig. 4. Capacity decay over cycle count (full cycle equivalent)

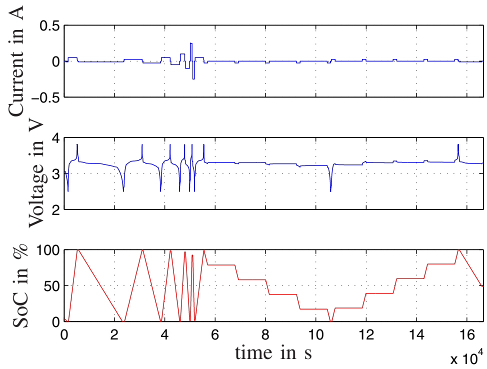

Fig. 5. Reference test of the new cell ($C_{act}/C_{init} = 1$)

In Fig. 5 the measured signals from the reference test of the new cell (i. e. the currently available capacity C_{act} of the cell is equal to the nominal capacity C_{init}) is depicted.

Please refer to [11] for a more detailed description of the experiment design of the cycling load and reference tests.

B. Cell modelling and interpretation of the LMNs

Each of the 17 reference tests is now used to create a new LMN. As described in the previous section, the model output is the cell terminal voltage and the inputs are the cell current and SoC. Note that SoC is regarded as an input for the training of the model, while for the observer design SoC is a state of the system, resulting in an augmented state space representation of the nonlinear battery model (please see also [10]).

As a first step, the interpretability of LMNs is used to extract information on the steady state gain and the relationship between open-circuit voltage (OCV) and SoC. In Fig. 6 the OCV-SoC relationship for each of the 17 models is depicted. Here the blue line represents the model of the new cell and the red line is obtained from the reference test at the end of the ageing experiment. Obviously, the decrease in capacity is directly visible from the extracted OCV-SoC curve.

In Fig. 7 the steady state gain (which is closely related to the internal resistance of the cell) of the 17 different LMNs is depicted:

$$K_I = \lim_{z\to 1} \left. \frac{\partial U}{\partial I} \right|_{SOC=const.} \tag{8}$$

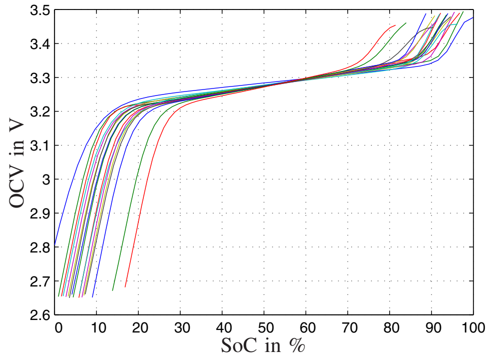

Fig. 6. OCV-SoC relationship for 17 reference tests each representing a different stage of the ageing process (blue = new, ..., red = old)

Again the blue line represents the new cell and the red line is obtained from the data measured at the end of the ageing experiment. Accordingly, the different characteristics in Fig. 7 reflect the increase in internal resistance.

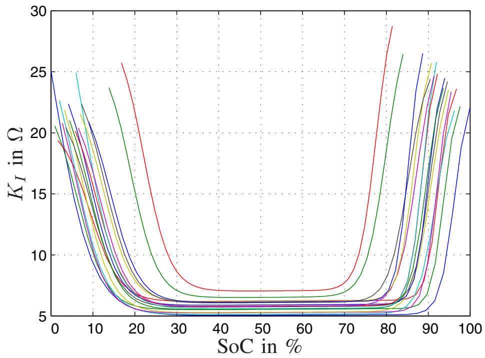

Fig. 7. Steady state gain for 17 reference tests each representing a different stage of the ageing process (blue = new, ..., red = old)

As a second step, the extracted characteristics are rescaled in a way such that the actual age (i. e. the currently available capacity of the cell, c. f. Fig. 3) is taken into account. In Fig. 8 the modified OCV-SoC relationship is depicted where the normalised/rescaled SoC is obtained from $SoC_{norm} = SoC\frac{C_{init}}{C_{act}}$. Apparently, the 17 OCV-SoC curves match almost perfectly although all LMNs (i. e. the local model parameters and the partitioning) were constructed independently (using different data records).

The resistance increase is taken into account using $K_{I,norm} = K_I \frac{C_{act}}{C_{init}}$. Fig. 9 depicts the *rescaled* relationship for the steady state gain where additionally the normalised state of charge $SoC_{norm} = SoC\frac{C_{init}}{C_{act}}$ is taken into account. Again, using only one parameter a good match between the different LMNs is obtained.

In Fig. 10 and Fig. 11 the effect of the model adaptation (i. e. the rescaling) is highlighted again by means of the OCV-SoC relationship. In addition to Fig. 6 and Fig. 8 also the calendrical age of the cell is directly visible in these figures.

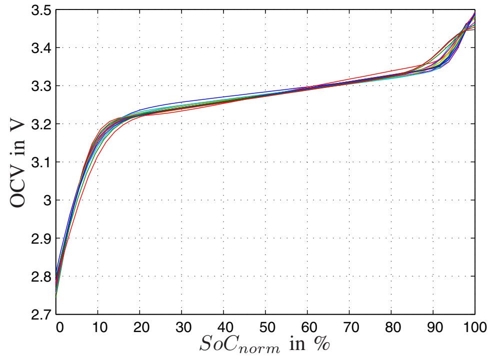

Fig. 8. OCV over *normalised* SoC for 17 LMNs

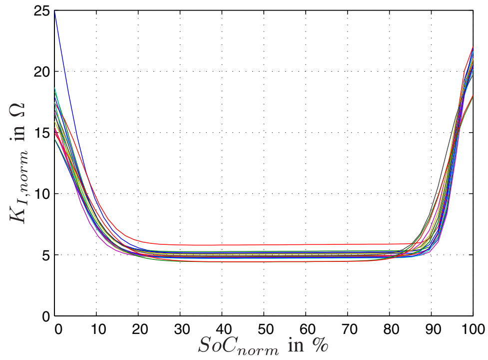

Fig. 9. *Rescaled* steady state gain over *normalised* SoC for 17 LMNs

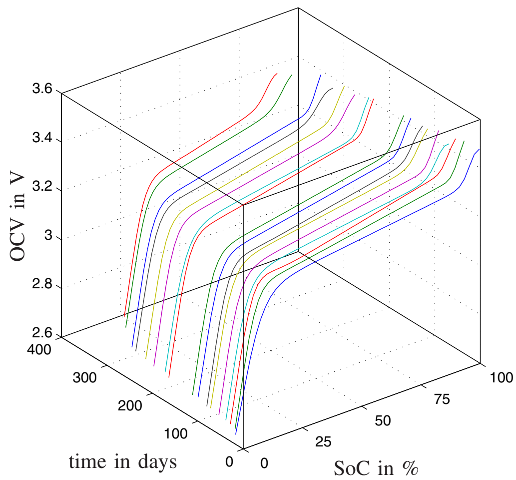

Fig. 10. Open-circuit voltage over time and SOC

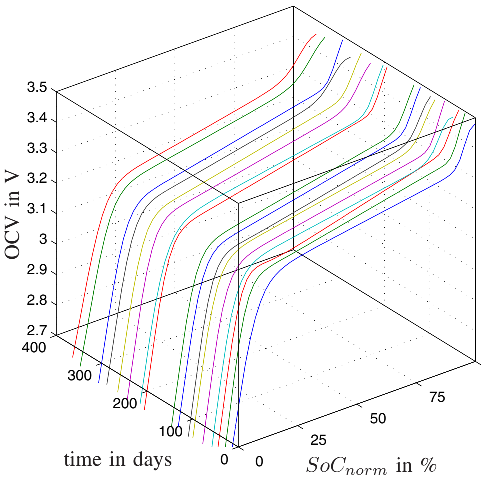

Fig. 11. Open-circuit voltage over time and *normalised* SOC

IV. Model adaptation

In this section the findings/ideas presented in Section III are used to adapt the data driven battery model. The resulting *time-variant* model allows to consider age-related effects. Thus, one LMN is constructed using data of the new cell and only a few parameters are used to adapt the LMN such that it can be used to predict/simulate the nonlinear dynamic behaviour of the cell at any stage of the ageing process. In the present application even only one parameter (i. e. the currently available capacity of the cell which is assumed to be known) is used to adapt the black-box model.

The simulation results without model adaptation (time-invariant LMN) using three different reference tests (at $C_{act}/C_{init} = 1$, $C_{act}/C_{init} = 0.84$ and $C_{act}/C_{init} = 0.63$, respectively) are depicted in Fig. 12. Apparently, the performance of the model decreases with the age-related capacity loss of the cell.

Fig. 13 shows the performance of the LMN without adaptation at all reference cycles by means of the R^2 statistics

$$R^2 = 1 - \frac{\sum_{k=1}^{N} (y(k) - \hat{y}(k))^2}{\sum_{k=1}^{N} (y(k) - \bar{y})^2}. \tag{9}$$

As expected, the capacity decay and resistance increase affect the simulation performance and the LMN (created with data of the new cell) insufficiently predicts the terminal voltage of the aged cell (c. f. Fig. 3).

In Fig. 14 a comparison of the LMN without adaptation to three different variants for model adaptation is presented:

(A) *Without adaptation:* Time-invariant model (see Fig. 13 and Fig. 12).
(B) *Corrected gain:* The steady state gain of the local linear models is adapted, see also Fig. 9.
(C) *Normalised SoC:* The SoC is rescaled, see also Fig. 8.
(D) *Rescaling of SoC and steady state gain:* Combination of (B) and (C) – i. e. SoC is rescaled and the steady state gain is adapted based on the age-related capacity decay.

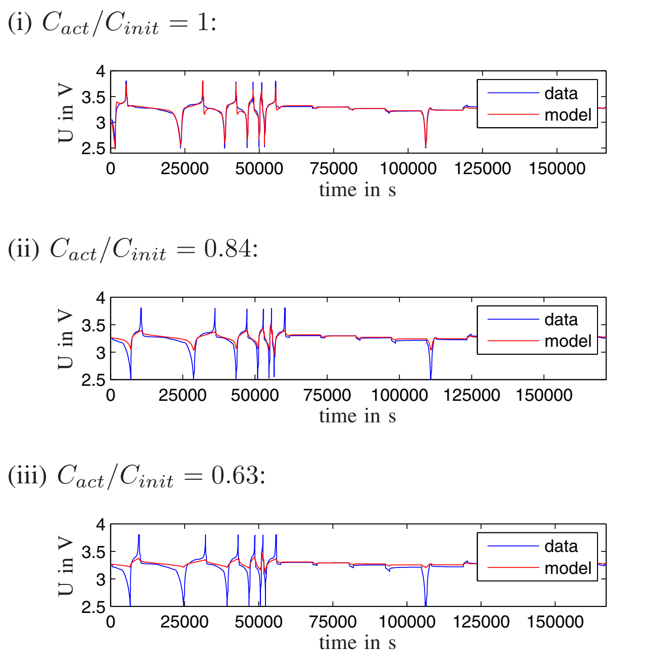

Fig. 12. Simulation of ageing data without model adaptation (time-invariant LMN)

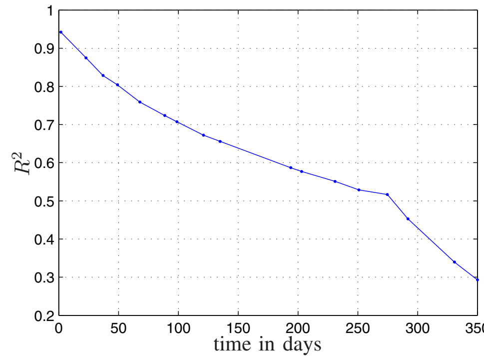

Fig. 13. Simulation of ageing data without model adaptation (time-invariant LMN)

Obviously, rescaling SoC and the steady state gain helps to improve the simulation performance significantly. Using the time-variant model (D) the LMN can be used to simulate the battery voltage at different stages of the ageing process almost without any loss of performance. Thus, using only one adaptation parameter, a simple but effective method for battery model adaptation is obtained.

The simulation results of the adapted LMN (D) for three different reference tests (at $C_{act}/C_{init} = 1$, $C_{act}/C_{init} = 0.84$ and $C_{act}/C_{init} = 0.63$, respectively) are depicted in Fig. 15.

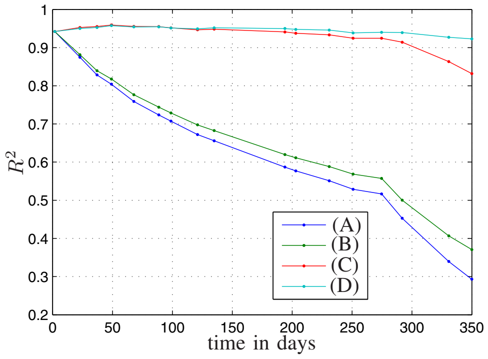

Fig. 14. Comparison of three different variants for model adaptation and the model without adaptation

(i) $C_{act}/C_{init} = 1$:

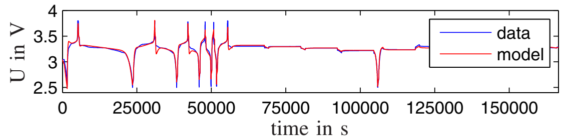

(ii) $C_{act}/C_{init} = 0.84$:

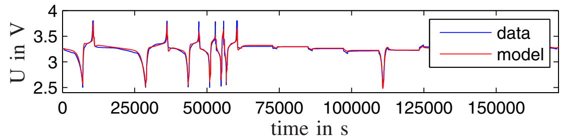

(iii) $C_{act}/C_{init} = 0.63$:

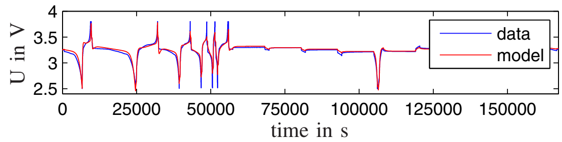

Fig. 15. Simulation of ageing data with model adaptation (time-variant model)

V. Conclusions and Outlook

The model based analysis of Lithium Ion cell ageing data and the age-related adaptation of the battery model is discussed in this paper. First, the interpretability of LMNs was used to extract information on the steady state gain and the relationship between OCV and SoC. Then, the extracted characteristics were rescaled in a way such that the actual age (i. e. the currently available capacity of the cell which was assumed to be known) is taken into account. Based on these findings, the adaptation of the data driven model was presented in order to consider age-related effects. The simulation results indicated that the resulting time-variant LMN allows to predict the battery voltage at any stage of the ageing process almost without any loss of performance.

Future research will be focused on the design of a combined observer for SoH and SoC. Based on the ideas presented in this paper, only one parameter (the currently available capacity of the cell) has to be adapted and thus estimated online (in addition to SoC) in order to take ageing into account.

References

[1] A. Vasebi, M. Partovibakhsh, and S. M. T. Bathaee, "A novel combined battery model for state-of-charge estimation in lead-acid batteries based on extended kalman filter for hybrid electric vehicle applications," *Journal of Power Sources*, vol. 174, no. 1, pp. 30 – 40, 2007, hybrid Electric Vehicles.

[2] A. Vasebi, S. Bathaee, and M. Partovibakhsh, "Predicting state of charge of lead-acid batteries for hybrid electric vehicles by extended kalman filter," *Energy Conversion and Management*, vol. 49, no. 1, pp. 75 – 82, 2008.

[3] J. Han, D. Kim, and M. Sunwoo, "State-of-charge estimation of lead-acid batteries using an adaptive extended kalman filter," *Journal of Power Sources*, vol. 188, no. 2, pp. 606 – 612, 2009.

[4] B. Bhangu, P. Bentley, D. Stone, and C. Bingham, "Nonlinear observers for predicting state-of-charge and state-of-health of lead-acid batteries for hybrid-electric vehicles," *Vehicular Technology, IEEE Transactions on*, vol. 54, no. 3, pp. 783 – 794, may 2005.

[5] G. L. Plett, "Extended Kalman filtering for battery management systems of LiPB-based HEV battery packs: Part 2. Modeling and identification," *Journal of Power Sources*, vol. 134, no. 2, pp. 262 – 276, 2004.

[6] S. Santhanagopalan and R. E. White, "Online estimation of the state of charge of a lithium ion cell," *Journal of Power Sources*, vol. 161, no. 2, pp. 1346 – 1355, 2006.

[7] I.-S. Kim, "The novel state of charge estimation method for lithium battery using sliding mode observer," *Journal of Power Sources*, vol. 163, no. 1, pp. 584 – 590, 2006, special issue including selected papers presented at the Second International Conference on Polymer Batteries and Fuel Cells together with regular papers.

[8] D. Andre, C. Appel, T. Soczka-Guth, and D. U. Sauer, "Advanced mathematical methods of {SOC} and {SOH} estimation for lithium-ion batteries," *Journal of Power Sources*, vol. 224, no. 0, pp. 20 – 27, 2013.

[9] B. Bhangu, P. Bentley, D. Stone, and C. Bingham, "Observer techniques for estimating the state-of-charge and state-of-health of vrlabs for hybrid electric vehicles," in *Vehicle Power and Propulsion, 2005 IEEE Conference*, 2005, pp. 10 pp.–.

[10] C. Hametner and S. Jakubek, "State of charge estimation for Lithium Ion cells: Design of experiments, nonlinear identification and fuzzy observer design," *Journal of Power Sources*, vol. 238, no. 0, pp. 413 – 421, 2013.

[11] W. Prochazka, G. Pregartner, and M. Cifrain, "Design-of-Experiment and Statistical Modeling of a Large Scale Aging Experiment for Two Popular Lithium Ion Cell Chemistries," *Journal of The Electrochemical Society*, vol. 160, no. 8, pp. A1039–A1051, Jan. 2013.

[12] R. Murray-Smith and T. A. Johansen, *Multiple Model Approaches to Modelling and Control*. Taylor & Francis, 1997.

[13] G. Gregorcic and G. Lightbody, "Local model network identification with gaussian processes," *Neural Networks, IEEE Transactions on*, vol. 18, no. 5, pp. 1404 –1423, sep. 2007.

[14] C. Hametner and M. Nebel, "Operating regime based dynamic engine modelling," *Control Engineering Practice*, vol. 20, no. 4, pp. 397 – 407, 2012.

[15] C. Hametner and S. Jakubek, "Local model network identification for online engine modelling," *Information Sciences*, vol. 220, no. 0, pp. 210 – 225, 2013, online Fuzzy Machine Learning and Data Mining.

[16] C. Hametner, J. Unger, and S. Jakubek, "Local Model Network based Dynamic Battery Cell Model Identification," in *Proceedings of the 12th WSEAS International Conference on robotics, control and manufacturing technology (ROCOM'12)*, April 2012.

[17] C. M. Bishop, *Neural networks for pattern recognition*. USA: Oxford University Press, 1995.

[18] P. Pucar and M. Millnert, "Smooth hinging hyperplanes - an alternative to neural networks," in *Proceedings of the 3rd ECC*, 1995.

[19] C. Hametner and S. Jakubek, "Neuro-fuzzy modelling using a logistic discriminant tree," *American Control Conference, 2007. ACC '07*, pp. 864–869, July 2007.